



NLR-TP-2004-166

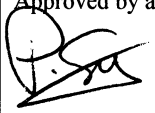
Identification of Noise Sources on Civil Aircraft in Approach using a Phased Array of Microphones

P. Sijtsma and H.M.M. van der Wal

This report has been based on a paper presented at NATO-RTO SET Symposium on "Capabilities of Acoustics in Air-Ground and Maritime Reconnaissance, Target Classification and -Identification", at Lercini, Italy on 26-28 April, 2004.

This report may be cited on condition that full credit is given to NLR and the authors.

Customer: National Aerospace Laboratory NLR
Working Plan number: AV.1.C.1
Owner: National Aerospace Laboratory NLR
Division: Aerospace Vehicles
Distribution: Limited
Classification title: Unclassified
April 2004

Approved by author:  14/5/04	Approved by project manager:  4/6/04	Approved by project managing department:  15/6
--	--	--



Contents

1	Introduction	4
2	Test set-up	5
3	Array Processing	6
3.1	Source description	6
3.2	Delay-and-Sum beamforming	7
3.3	Source power spectra	7
3.4	Weight factors	8
4	Array design	8
4.1	Requirements	8
4.2	Loss of coherence	8
4.3	Resolution	10
4.4	Properties	10
5	Aircraft Tracking	11
5.1	Light sensors	11
5.2	Laser plus Inertial Measuring Unit	11
5.3	Video	12
5.4	Comparison between tracking techniques	12
6	Conclusion	13
7	Acknowledgement	14
8	References	14

12 Figures

(14 pages in total)



Identification of Noise Sources on Civil Aircraft in Approach using a Phased Array of Microphones

Dr. ir. Pieter Sijtsma & Ir. Henk M.M. van der Wal

National Aerospace Laboratory NLR
Department of Helicopters & Aeroacoustics
P.O. Box 153
8300 AD Emmeloord
The Netherlands
E-mail: sijtsma@nlr.nl / vdwal@nlr.nl

SUMMARY

In September 2002, microphone array measurements were performed on landing aircraft at Amsterdam Airport Schiphol. During three days of measurements, 484 fly-over events were recorded successfully. Many aircraft types were included. Most fly-overs were recorded with a large array of 243 microphones. Using a convenient source description, which includes the effect of Doppler frequency shift, acoustic images were obtained through Delay-and-Sum beamforming. The array consisted of a number of concentric rings of microphones. Maximum resolution was achieved by applying weight factors that correct for microphone spatial density. Furthermore, frequency-dependent spatial windowing was applied to account for the effects of coherence loss. Herewith, the lobe widths were constant for a large range of frequencies. The speed and the altitude of the airplanes were determined by a set of light sensors. This light sensor technique enabled an efficient, automatic determination of speed and height, without the cumbersome manual processing that is needed with for instance video cameras.

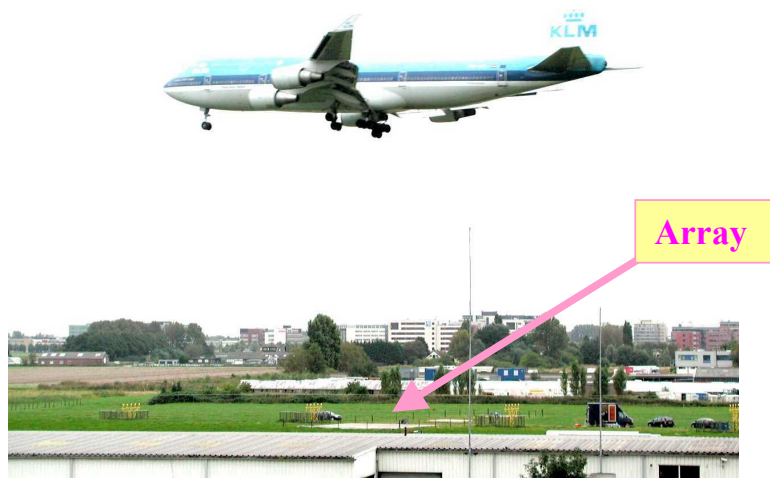


Figure 1: Array measurements at Schiphol Airport

Identification of Noise Sources on Civil Aircraft in Approach

1. INTRODUCTION

In the last decade, microphone arrays have become more and more in use as a standard tool for acoustic source location. The increasing capacity of computers and data acquisition systems have enabled the use of large numbers of microphones, long acquisition times and high sample frequencies [1]. Microphone arrays can be applied to stationary sources, but also to moving sources. Sound source location on moving objects has been applied to rotating sources in wind tunnels [2], to trains passing by [3],[4], and to aircraft flying over [5]-[7].

Aircraft fly-over array measurements can be used to investigate the noise of individual airframe noise components and to assess the model scale effects of wind tunnel measurements [7]. Moreover, fly-over array measurements can be valuable for making a breakdown of all possible noise sources, including engine noise, so that their relative contributions to the total noise perceived on the ground is known.



Figure 2: Platform with microphone array

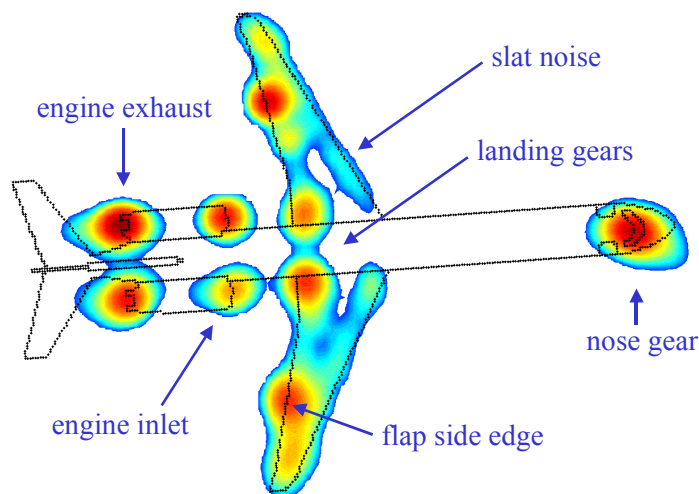


Figure 3: Acoustic image of an MD82 aircraft; 1600 Hz 1/3 octave band



Identification of Noise Sources on Civil Aircraft in Approach

In September 2002, NLR performed microphone array measurements on landing aircraft at Amsterdam Airport Schiphol (see Figure 1). During three days of measurements, 484 fly-over events were recorded successfully. The average fly-over altitude above the array was 43 m; the average speed was 68 m/s. Many aircraft types were included. Most fly-over events were recorded with an array of 243 microphones, which were located within a circle of 6 m radius. The array was mounted on a wooden platform (see Figure 2)

The measurements did not only provide an extensive data set of aircraft noise sources (see for example the acoustic image of an MD82 aircraft in Figure 3), but also information on the array measurement technique itself, including possibilities for future improvements. One of these envisaged future improvements is the development of a technique to determine absolute contributions of aircraft noise components [8].

In this paper, we will give a brief impression of the test site and the measurement equipment. In more detail, a description is given of the array procession technique, and, closely connected, the array design. Finally, the aircraft tracking technique by means of light sensors is discussed.

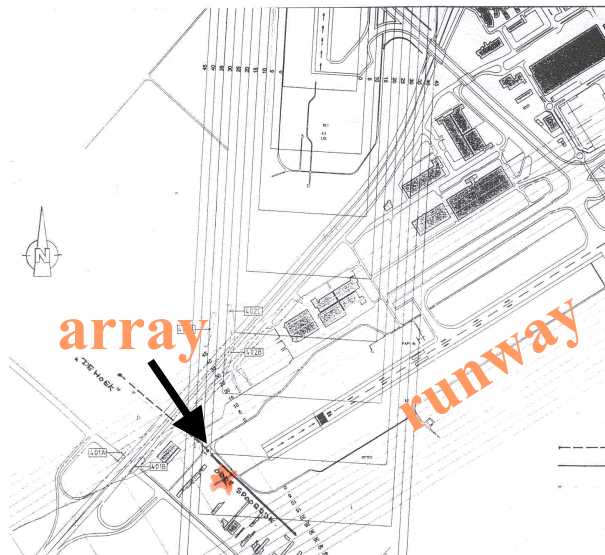


Figure 4: Ground plan of the test site

2. TEST SET-UP

The microphone array was located at a distance of about 750 m from the threshold of the “Kaagbaan” runway. Figure 4 shows a general ground plan of the test site and surroundings. In Figure 5, a detailed layout of the test terrain is shown. The flight direction for landing aircraft is from left to right. In the following, the measurement equipment is summarised.

- 243 microphones were mounted on a platform of $13.42 \times 13.42 \text{ m}^2$ (see Figure 2). The midpoint of the array was located at 8 m distance from the extended runway centre line (“ground track” in Figure 5).
- 5 light sensors were placed at the line $y = 8 \text{ m}$, i.e., at the same distance from the extended runway centre line as the array centre. Three of them, located at $x = -50 \text{ m}$, $x = +10 \text{ m}$ and $x = +50 \text{ m}$, were directed perpendicular upwards (90°). The other two sensors, located at $x = -10 \text{ m}$ and $x = -50 \text{ m}$, had an elevation of 45° with respect to the “upstream” horizon.



Identification of Noise Sources on Civil Aircraft in Approach

- A “laser plus IMU” (Inertial Measuring Unit) system, and a video camera directed 90° upwards were placed near the origin in Figure 5.

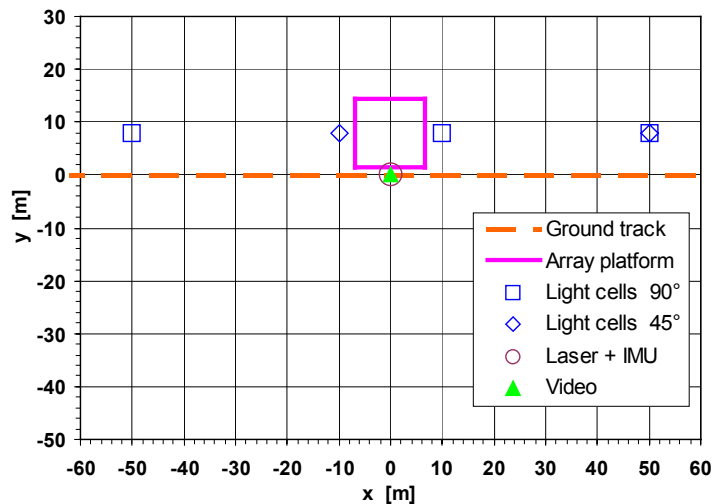


Figure 5: Test terrain layout

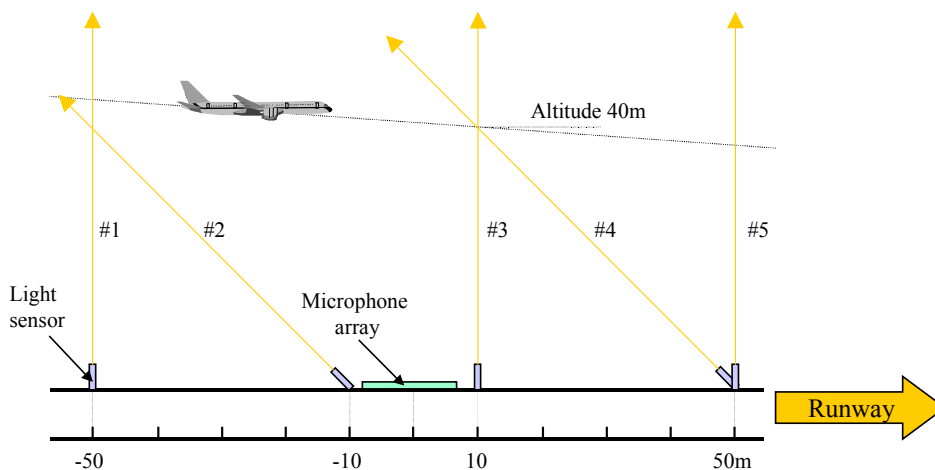


Figure 6: Positions and orientations of the light sensors

3. ARRAY PROCESSING

3.1 Source description

The beamforming algorithm that we used is based on the following sound transfer description from a moving sound source above the array to the microphones on the ground.

Suppose that a point source moves with time-dependent position $\vec{\xi}(t)$, while emitting a sound signal $\sigma(t)$. The N microphones on the ground, located in \vec{x}_n , $n=1, \dots, N$, record the induced acoustic pressures



Identification of Noise Sources on Civil Aircraft in Approach

$\chi_n(t)$. The relation between emitted and measured sound is:

$$\chi_n(t_n) = T_n(t_n, \tau) \sigma(\tau), \quad (1)$$

where τ is the emission time and t_n is the microphone-dependent receiving time. The transfer function T_n , which is based on a sound field description of a monopole source moving in a homogeneous atmosphere at rest [9], is given by

$$T_n(t_n, \tau) = 1/4\pi \left\{ \|\bar{x}_n - \bar{\xi}(\tau)\| - \frac{1}{c} \bar{\xi}'(\tau) \cdot (\bar{x}_n - \bar{\xi}(\tau)) \right\}, \quad (2)$$

where c is the speed of sound. The relation between emission and receiving time is:

$$t_n - \tau = \frac{1}{c} \|\bar{x}_n - \bar{\xi}(\tau)\|. \quad (3)$$

This source description includes the Doppler frequency shift.

3.2 Delay-and-Sum beamforming

A source signal $\tilde{\sigma}(\tau)$ can be reconstructed from (1) with the Delay-and-Sum procedure:

$$\tilde{\sigma}(\tau) = \frac{1}{N} \sum_{n=1}^N \tilde{\sigma}_n(\tau), \quad (4)$$

where

$$\tilde{\sigma}_n(\tau) = \chi_n(t_n) / T_n(t_n, \tau). \quad (5)$$

Clearly, when the moving focus $\bar{\xi}(t)$, i.e., the assumed source path that is used to calculate T_n , coincides with an actual moving monopole source, we find $\tilde{\sigma}(\tau) = \sigma(\tau)$. If there is a mismatch between moving focus and moving source, we usually have $|\tilde{\sigma}(\tau)| < |\sigma(\tau)|$.

3.3 Source power spectra

A straightforward way to calculate the frequency spectrum of a source signal is evaluating Eq. (4) for $\tau = k\Delta t$, $k = 1, \dots, K$, and then performing a discrete Fourier transform (DFT):

$$\tilde{\mathfrak{S}}(\tilde{\sigma}) = \frac{1}{N} \sum_{n=1}^N \tilde{\mathfrak{S}}(\tilde{\sigma}_n). \quad (6)$$

The DFT result $\tilde{\mathfrak{S}}$ is written here in vector notation. The individual components \mathfrak{S}_j are the spectral results at the frequencies:

$$f_j = j/\Delta t, j = 1, \dots, \frac{1}{2}K - 1 \quad (7)$$



Identification of Noise Sources on Civil Aircraft in Approach

The source power spectrum is calculated as follows:

$$\frac{1}{2} |\mathfrak{S}_j(\tilde{\sigma})|^2 = \frac{1}{2N^2} \left| \sum_{n=1}^N \mathfrak{S}_j(\tilde{\sigma}_n) \right|^2 = \frac{1}{2N^2} \sum_{n=1}^N \sum_{m=1}^N \mathfrak{S}_j(\tilde{\sigma}_n) \mathfrak{S}_j(\tilde{\sigma}_m)^*, \quad (8)$$

in which the asterisk denotes complex conjugation. If the microphone signals suffer from relatively high incoherent noise levels (e.g. wind noise), then the following approximation of (8) may be considered

$$\frac{1}{2} |\mathfrak{S}_j(\tilde{\sigma})|^2 = \frac{1}{2N(N-1)} \sum_{n=1}^N \sum_{\substack{m=1 \\ m \neq n}}^N \mathfrak{S}_j(\tilde{\sigma}_n) \mathfrak{S}_j(\tilde{\sigma}_m)^* = \frac{1}{2N(N-1)} \left(\left| \sum_{n=1}^N \mathfrak{S}_j(\tilde{\sigma}_n) \right|^2 - \sum_{n=1}^N |\mathfrak{S}_j(\tilde{\sigma}_n)|^2 \right). \quad (9)$$

3.4 Weight factors

It is possible to apply n -dependent weight factors $w_{j,n}$ (i.e., a spatial window), in the foregoing estimations of source power spectra. These weights may be frequency (j) dependent. Equations (8) then changes into:

$$\frac{1}{2} |\mathfrak{S}_j(\tilde{\sigma})|^2 = \frac{1}{2} \sum_{n=1}^N \sum_{m=1}^N w_{j,n} w_{j,m} \mathfrak{S}_j(\tilde{\sigma}_n) \mathfrak{S}_j(\tilde{\sigma}_m)^* / \sum_{n=1}^N \sum_{m=1}^N w_{j,n} w_{j,m} \quad (10)$$

4. ARRAY DESIGN

4.1 Requirements

The array was designed to have good performance in the frequency range 500 – 6000 Hz. In this range the array is required to have high array gain (low side lobe levels) and high resolution (narrow beam widths). The maximum radius for the microphone array was 6 m. The number of data channels available for microphones was 243.

4.2 Loss of coherence

In a previous measurement campaign at Schiphol Airport (September 2000) it was found that the array resolution is limited by loss of coherence due to atmospheric turbulence [10],[11]. During propagation from noise sources on the aircraft to microphones on the ground, the sound signals are distorted by turbulence. This distortion is different from microphone to microphone, which results in loss of coherence between the different microphone signals. Loss of coherence becomes more significant for increasing distance between microphones, and for increasing frequency. For high frequencies, the outer microphones of the array have become completely incoherent with the other microphones, and thus the effective aperture of the array has become smaller than its physical size.

Quantifying the coherence loss is difficult. In the literature, there is no description of coherence loss of sound that propagates in vertical direction through the atmosphere. Also, it can not be deduced immediately from the fly-over measurements. Assessment of coherence loss would have been possible through single source measurements at an altitude of 40 m above the array, but such a test would incur practical problems (e.g. at the test site it would be impossible, for safety reasons).

Loss of coherence can be perceived indirectly from the fly-over measurements. This can be done by processing array data of a single fly-over event with different array sizes [12], and comparing the resultant acoustic images. First, an array processing can be done with the entire array, and then the outer part of the



Identification of Noise Sources on Civil Aircraft in Approach

array can be excluded from the processing. If the outer microphones are affected by loss of coherence, they do not contribute effectively to the beamforming process, but they only add noise. Reduction of array size will then not result into lower resolution. Instead, the peak levels will increase and the noise levels in the acoustic images will decrease.

By performing such a study with different array sizes, using data from the previous Schiphol measurement campaign, it was found that the radius of the effective array aperture is, approximately:

$$R_j = 4000/f_j . \tag{11}$$

In other words, the effective array aperture at 4000 Hz is approximately a disk of 1 m radius. At other frequencies the effective array aperture is inverse proportional to the frequency.

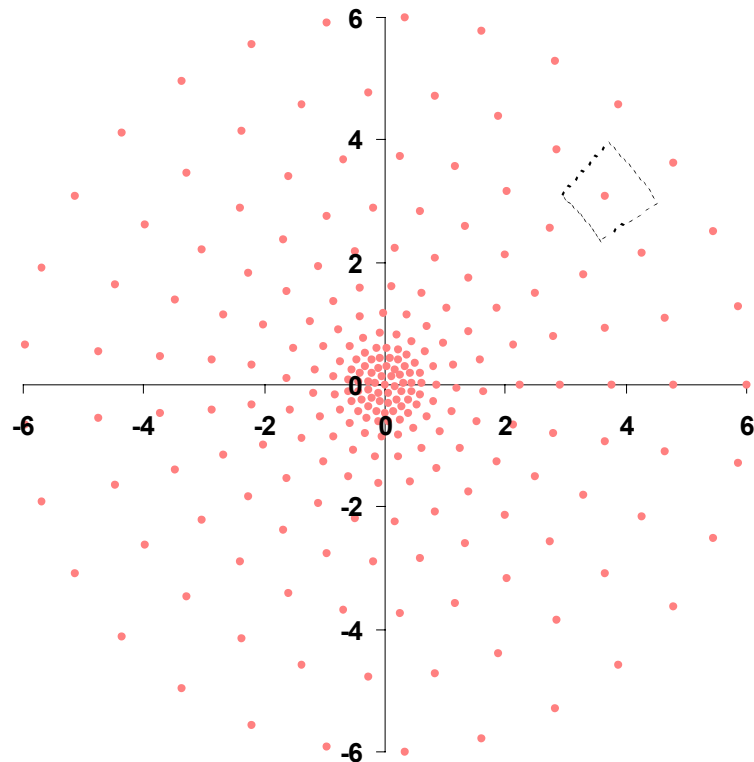


Figure 7: Microphone layout & area association

In order to have high array gain at the entire frequency range of interest, it is required to have available a sufficiently large number of microphones for each frequency. This holds in particular for the highest frequencies, where the effective array aperture (11) is small. Therefore, an array design was made with a high microphone density in the central part of the array, and more sparsely spaced microphones in the periphery (see Figure 7).

The effects of frequency-dependent effective array apertures were incorporated in the beamforming process, by applying the following weight factors (see Section 3.4):



Identification of Noise Sources on Civil Aircraft in Approach

$$w_{n,j} = \Omega\left(\frac{r_n}{R_j}\right) = \frac{1}{2} \left\{ 1 - \text{Erf} \left[8 \left(\frac{r_n}{R_j} - 1 \right) \right] \right\}, \quad (12)$$

where ‘Erf’ is the Error function and r_n is the distance to the midpoint of the array. The “spatial window” function Ω is illustrated in Figure 8.

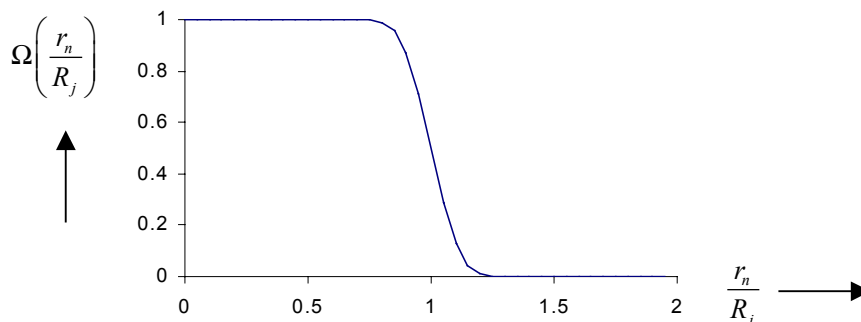


Figure 8: Illustration of Eq. (12)

4.3 Resolution

A drawback of an array design with densely spaced microphones in the central part, and more sparsely spaced microphones in the outer part, is that the array resolution is not optimal. If all microphones are processed with the same weight (using the weight factors (12), this happens for $R_j > 6$ m, hence for $f < 667$ Hz), then too much emphasis is put on the central part. Consequently, the array resolution is less than the resolution of a comparable continuous disk (or elliptic mirror) of the same size.

The above-mentioned drawback can be countered by associating each microphone (n) with a surrounding area, say λ_n^2 (m²). These areas can be incorporated in the weight factors (12) as follows:

$$w_{n,j} = \lambda_n \Omega\left(\frac{r_n}{R_j}\right) = \frac{1}{2} \lambda_n \left\{ 1 - \text{Erf} \left[8 \left(\frac{r_n}{R_j} - 1 \right) \right] \right\}. \quad (13)$$

The weights λ_n are such that the processed acoustic power per unit area is approximately constant.

The array design (Figure 7) is such that this microphone-dependent area association is indeed possible. The array is built up by a number of concentric rings with increasing spacing towards the outer part. The spacing between rings is kept, as much as possible, the same as the spacing between two adjacent microphones in a ring. Thus, an area association is straightforward, as illustrated in Figure 7.

4.4 Properties

Using the beamforming algorithm of Section 3, with the weight factors (13), the array design has the following properties:

- Below 6300 Hz, the dynamic range (difference between peak level and highest side lobe level) is about 12 dB, in a scanning area of 80×80 m², 40 m above the array.



Identification of Noise Sources on Civil Aircraft in Approach

- Due to the frequency-dependent spatial windowing (13), the lobe widths are constant for a large range of frequencies. For 667 Hz and higher, the spatial resolution of the array (see Figure 9) is 2 m, at 40 m altitude. Below 667 Hz, the resolution is inverse proportional to the frequency.

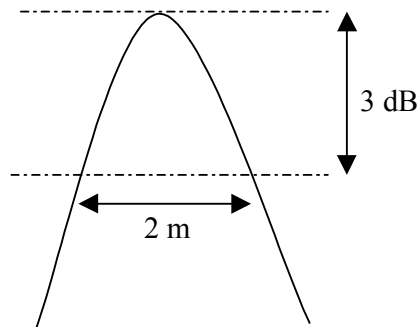


Figure 9: Definition of array resolution

5. AIRCRAFT TRACKING

5.1 Light sensors

Because of the large number of fly-over events, it was desired to have available a system that determines aircraft speed and altitude automatically, i.e., without the cumbersome manual processing that is needed with video cameras or laser systems. Therefore, a tracking system was developed using 5 passive light sensors mounted in tubes, 3 of which are pointing vertically (90°), and two of which point at 45° (see Figure 6). The AC-components of the sensor output signals were recorded simultaneously with the microphones.

The signals from the different sensors were well correlated, as can be seen in the example of Figure 10. Therefore the time difference between the sensor signals, in other words, the differences in time that the airplane passes the beams, can be calculated automatically. This was done by a cross-correlation analysis, viz. by searching the maximum values of the cross-correlation functions. The ground speed was determined using the signals of the three 90° sensors, the altitude was determined on two locations using the additional information from the 45° sensors.

5.2 Laser plus Inertial Measuring Unit

As back-up for the light sensors, a hand-held laser distance measurement unit was used to measure the distance from an observer to the aircraft. At a distance of about 200 m the laser picked up the aircraft at a point underneath the nose of the fuselage. This point was tracked until the aircraft flew overhead and beyond. The minimum distance observed is the altitude of the aircraft above the observer.

An IMU (Inertial Measurement Unit) was fixed to the hand held laser enabling the measurement of the pitch angle of the laser unit. The combined information of the laser distance and the pitch angle enabled to track the aircraft altitude and horizontal speed over a distance of about 200 m. The hand-held laser plus IMU were located near the origin (see Figure 5).



Identification of Noise Sources on Civil Aircraft in Approach

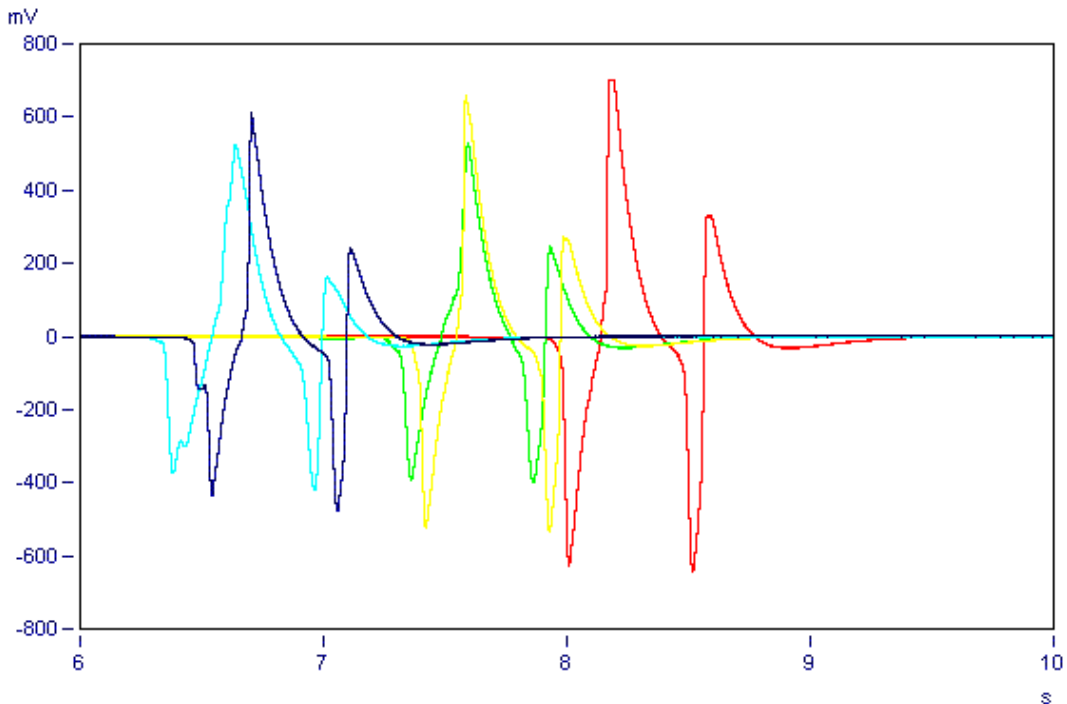


Figure 10: Signals from light sensors from a single fly-over event

5.3 Video

Video cameras were used as back-up for the laser/IMU combination and the light sensors. Three video camcorders were installed: The first camera, which was directed 90° upwards, was placed next to the platform (depicted in Figure 5). The second camera was placed at the extended runway centre line ($x = -102.5$ m, $y = 0$ m), and directed towards a point 40 m above the origin. The third video camera was placed beside the centre line ($x = 0$ m, $y = -111.3$ m), and also directed towards a point 40 m above the origin. The positions of the second and the third camera were outside the range of Figure 5. From these three video registrations, the position of the aircraft as function of time could be computed. The pictures had to be calibrated in direction and scaled carefully.

5.4 Comparison between tracking techniques

For a limited number of fly-overs, a comparison was made between altitude and speed data obtained with the light sensors, the laser/IMU system and the video cameras. The results are shown in Figure 11 (altitude) and Figure 12 (speed).

The laser/IMU altitude results are, systematically, a few meters lower than the light sensor results. On the other hand, the lateral camera results are a few meters higher. Anyhow, the spreading of the results are all within the (vertical) dimensions of the airplanes.

The laser/IMU speed results are obtained by processing only the data between 150 m and 50 m before fly-over, because the overhead laser data were too inaccurate. Processed under this restriction, the laser/IMU results agree well with the light sensor results. Only for two flights (148 and 180) there is still a considerable difference, for which no explanation was found.



Identification of Noise Sources on Civil Aircraft in Approach

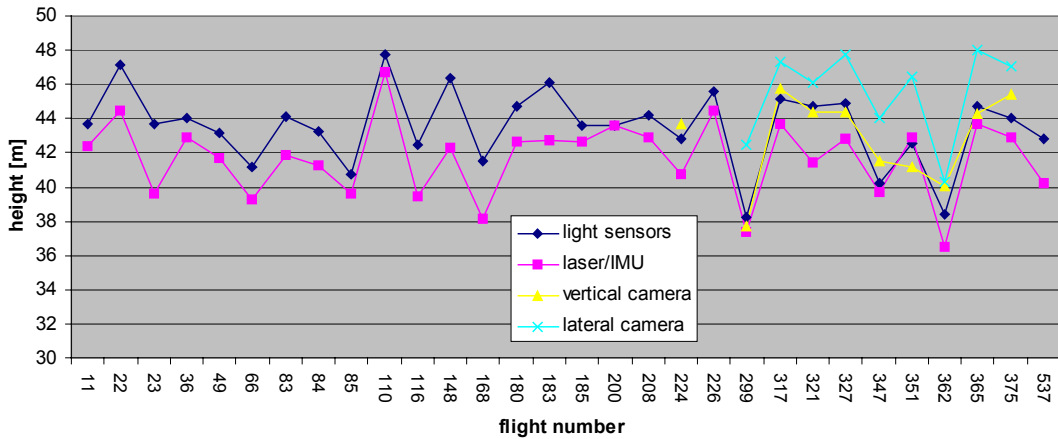


Figure 11: Aircraft fly-over altitude obtained by several techniques

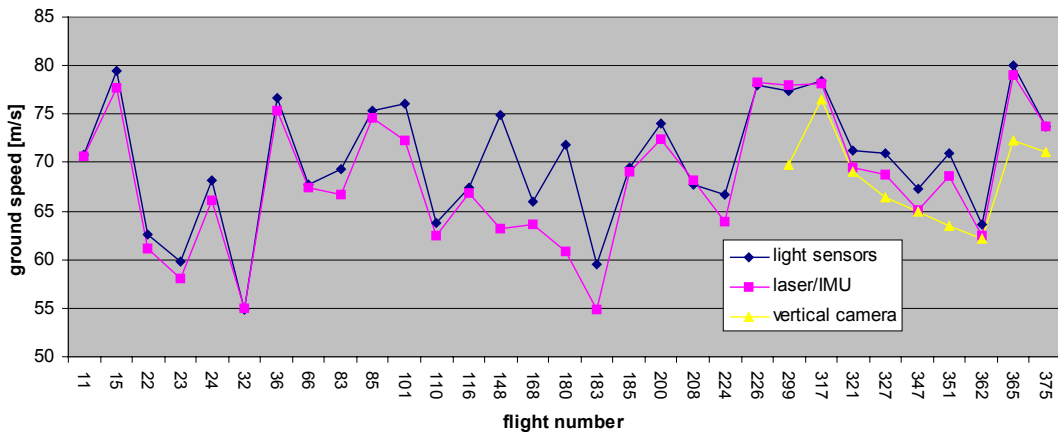


Figure 12: Aircraft ground speed obtained by several techniques

6. CONCLUSION

In September 2002, microphone array measurements were performed on landing aircraft at Amsterdam Airport Schiphol. In this paper, the following technical aspects of the array measurements have been discussed:

- Test set-up: A brief description was given of the test site and the measurement equipment.
- Array processing: Using a convenient source description, which includes the effect of Doppler frequency shift, acoustic images were obtained through Delay-and-Sum beamforming. The beamforming algorithm included microphone-dependent weight factors.
- Array design: The microphones were located on a number of concentric rings. Maximum array resolution was achieved by applying weight factors that correct for microphone spatial density. Furthermore, frequency-dependent spatial windowing was applied to account for the effective



Identification of Noise Sources on Civil Aircraft in Approach

(due to coherence loss) aperture of the array. Herewith, the lobe widths were constant for a large range of frequencies.

- Aircraft tracking: The speed and the velocity of the airplanes were determined by 5 light sensors. The sensor signals were processed automatically. The sensor results were compared with results from a hand-held laser system and from a set of video cameras, for which the data are much more time-consuming to process. The agreement was good.

7. ACKNOWLEDGEMENT

The measurements were performed under contract with Boeing Research & Technology Center, S.L. (Madrid, Spain).

8. REFERENCES

- [1] H.H. Holthusen, H. Smit, "A new data acquisition system for microphone array measurements in wind tunnels", AIAA Paper 2001-2169, 2001.
- [2] P. Sijtsma, S. Oerlemans, H.H. Holthusen, "Location of rotating sources by phased array measurements", AIAA Paper 2001-2167 (also NLR-TP-2001-135), 2001.
- [3] Y. Takano, K. Horihata, R. Kaneko, Y. Matsui, H. Fujita, "Analysis of sound source characteristics of Shinkansen cars by means of X-shaped microphone array", *Internoise 96*, Liverpool, 1996.
- [4] B. Barsikow, "Experiences with various configurations of microphone arrays used to locate sound sources on railway trains operated by the DB AG", *Journal of Sound and Vibration*, Vol. 193, No. 1, 1996, pp. 283-293.
- [5] U. Michel, B. Barsikow, J. Helbig, M. Hellmig, M. Schüttpelz, "Flyover noise measurements on landing aircraft with a microphone array", AIAA Paper 98-2336, 1998.
- [6] J.-F. Piet, U. Michel, P. Böhning, "Localization of the acoustic sources of the A340 with a large phased microphone array during flight tests", AIAA Paper 2002-2506, 2002.
- [7] R.W. Stoker, Y. Guo, C. Streett, N. Burnside, "Airframe noise source locations of a 777 aircraft in flight and comparisons with past model-scale tests", AIAA Paper 2003-3232, 2003.
- [8] P. Sijtsma, R.W. Stoker, "Determination of absolute contributions of aircraft noise components using fly-over array measurements", AIAA Paper 2004-2960, 2004.
- [9] A.P. Dowling, J.E. Ffowcs Williams, *Sound and Sources of Sound*, Wiley, 1983.
- [10] V.I. Tatarski, *Wave propagation in a Turbulent Medium*, McGraw-Hill, 1961.
- [11] R.P. Dougherty, "Turbulent decorrelation of aeroacoustic phased arrays: Lessons from atmospheric science and astronomy", AIAA Paper 2003-3200, 2003.
- [12] T. F. Brooks, W.M. Humphreys Jr., "Effect of directional array size on the measurement of airframe noise components", AIAA Paper 99-1958, 1999.